2019-07-01

Jurassic shift from abiotic to biotic control on marine ecological success

Eichenseer, K

10.1038/s41561-019-0392-9
Nature Geoscience
Nature Research

accepted on the 22nd of May 2019

Jurassic shift from abiotic to biotic control on marine ecological success

Kilian Eichenseer[1], Uwe Balthasar[1], Christopher W. Smart[1], Julian Stander[2], Kristian A. Haaga[3,4,5], Wolfgang Kiessling[6]

[1] School of Geography, Earth and Environmental Sciences, University of Plymouth, Drake Circus, Plymouth PL4 8AA, UK

[2] School of Computing, Electronics and Mathematics, University of Plymouth, Drake Circus, Plymouth PL4 8AA, UK

[3] Department of Earth Science, University of Bergen, N-5020 Bergen, Norway

[4] Bjerknes Centre for Climate Research, PO Box 7803, NO-5020 Bergen, Norway

[5] K.G. Jebsen Centre for Deep Sea Research, P.O. Box 7803, N-5020, Bergen, Norway

[6] GeoZentrum Nordbayern, Department of Geography and Geosciences, Universität Erlangen-Nürnberg, Loewenichstraße 28, 91054 Erlangen, Germany

Environmental change and biotic interactions both govern the evolution of the biosphere, but the relative importance of these drivers over geological time remains largely unknown. Previous work suggests that, unlike environmental parameters, diversity dynamics differ profoundly between the Palaeozoic and post-Palaeozoic eras. Here we use the fossil record to test the hypothesis that the influence of ocean chemistry and climate on the ecological success of marine calcifiers decreased throughout the Phanerozoic eon. Marine calcifiers build skeletons of calcite or aragonite, and the precipitation of these calcium carbonate polymorphs is governed by the magnesium-to-calcium ratio and temperature in abiotic systems. We developed an environmental forcing model based on secular changes of ocean chemistry and temperature and assessed how well the model predicts the proliferation of skeletal taxa with respect to calcium carbonate polymorphs. Abiotic forcing governs the ecological success of aragonitic calcifiers from the Ordovician to the Middle Jurassic, but not thereafter. This regime shift coincides with the proliferation of calcareous plankton in the mid-Mesozoic. The deposition of biomineralizing plankton on the ocean floor buffers CO_2 excursions and stabilizes Earth's biochemical cycle, and thus mitigates the evolutionary impact of environmental change on the marine biota.

Dramatic shifts in the success of dominant animal groups in Earth history abound in the fossil record[1] and there are numerous Phanerozoic-scale macroevolutionary trends. Traits such as body size, the metabolic rate of dominant taxonomic groups, and physiological buffering capacity have increased over the course of the Phanerozoic[2-5]. As a consequence, biotic interactions may have increased as well[6-9]. In contrast, climate and seawater composition show a cyclical behaviour rather than Phanerozoic-scale trends[10,11]. The biosphere has evolved to cushion some environmental variability: for example, the buffering of ocean

chemistry has increased due to the mid-Mesozoic ascent of calcifying plankton[12]. Perturbations of the carbon cycle have fallen in amplitude, particularly since the mid-Mesozoic[13] (Fig. 1d), and extinction rates have decreased towards the present[14] (Fig. 1e). Accordingly, we hypothesize that the evolutionary importance of the abiotic environment, relative to intrinsic, biotic factors, has declined through geological time.

We tested this hypothesis using the vast fossil record of marine calcifiers. In the inorganic formation of calcium carbonate ($CaCO_3$), high Mg/Ca ratios and high temperatures have been shown to favour the precipitation of aragonite over calcite, and *vice versa*[15]. Across the Phanerozoic, tectonically driven changes in sea water chemistry and climate have caused aragonite and calcite favouring conditions to alternate, giving rise to episodes of "aragonite seas" and "calcite seas"[10,16] (Fig. 1b). The skeletal mineralogy of calcifying organisms is strongly tied to phylogenetic history, but the *de novo* acquisition of biominerals, skeletal composition, skeletal production, and growth rates of many marine calcifiers are affected by the Mg/Ca ratio and temperature of the surrounding sea water[17-21], analogous to inorganic $CaCO_3$ formation. If aragonite and calcite seas were influential in the evolution of marine calcifiers, we expect a correspondence of aragonite sea conditions with greater success of aragonitic taxa.

Aragonite - calcite seas and the success of marine calcifiers

We combine a model of past Mg/Ca ratios[22] (Fig. 1b) with $\delta^{18}O$ temperature reconstructions[23] (Fig. 1c) to quantify *aragonite sea intensity* (*ASI*) in 85 post-Cambrian stages. The *ASI* is parametrized from experimental data[15] via multiple regression. We contrast *ASI* with a measure of the environmental occupancy, or success, of aragonitic genera relative to all calcifying genera ($SCOR_{ara}$), calculated with the Summed Common species Occurrence Rate

(SCOR)[24]. Given that novel acquisitions of calcium carbonate skeletons are rare and that switches in skeletal mineralogy are largely restricted to a few clades[20,21,25], changes in $SCOR_{ara}$ reflect predominantly the differential success of aragonitic taxa, rather than changing mineralogies within calcifying clades (Supplementary Materials S6). Although the lower preservation potential of aragonitic taxa may lead to underestimate the abundance of aragonitic taxa[26], we find that the completeness of the record of aragonitic and calcitic genera is not significantly different (Wilcoxon signed-rank test: $p = 0.28$, Supplementary Materials S3). The strength of abiotic controls on marine calcifiers is assessed by estimating linear models of $SCOR_{ara}$ against *ASI* using generalised least squares (GLS) to account for temporal autocorrelation, and by convergent cross mapping (CCM) to detect causal coupling[27] *(Methods).*

Visual inspection of the $SCOR_{ara}$ and *ASI* time series suggests an association in the Ordovician – Carboniferous and again in the early Mesozoic, but not for most of the Mesozoic and Cenozoic (Fig. 1a). A linear model of $SCOR_{ara}$ against *ASI* is significant in the Palaeozoic ($R^2 = 0.15$, $p = 0.017$, Table 1), and not in the Mesozoic – Cenozoic ($R^2 < 0.01$, $p = 0.68$), suggesting a decreasing dependence of ecological success on relevant environmental conditions in the Mesozoic. In the entire Ordovician – Pleistocene data, the linear relationship is not significant ($R^2 < 0.01$, $p = 0.70$), however the sharp rise of $SCOR_{ara}$ across the Permian-Triassic makes estimating linear models across this boundary problematic.

We used a Bayesian approach to identify the timing of the changes in the relationship between $SCOR_{ara}$ and *ASI* (see *Methods*). This analysis identifies the Permian-Triassic boundary as the strongest change point of the entire Phanerozoic time series (supported by 100 % posterior probability; Fig. 2a, purple bar). When evaluating only the Palaeozoic time

series, the Carboniferous – Permian boundary shows the strongest change (73% probability; Fig. 2a, red bars), whereas no unambiguous single change point is found for the Mesozoic – Cenozoic time series (all probabilities <25%; Fig. 2a, green bars).

To evaluate the possibility of a gradual change, we fitted linear models of $SCOR_{ara}$ against *ASI* from the Triassic onwards, adding successively more stages towards the present, and repeated the same process with the Palaeozoic data, separately. The relationship of $SCOR_{ara}$ and *ASI* is consistently strong in the Palaeozoic, with a weakening around the Carboniferous – Permian boundary (Figure 2b). In the Mesozoic, a positive linear relationship persists up to the Middle Jurassic, although with lower statistical support. No relationship is supported from the Late Jurassic onwards. The relationship of $SCOR_{ara}$ and *ASI* evolves in a similar way when $SCOR_{ara}$ is calculated only in the subset of organisms which are considered especially responsive to physiochemical changes in the environment (Supplementary Fig. S7)[2,25,28].

These results are reinforced by using CCM, a technique developed to detect causal coupling between time series by quantifying the extent to which a putative response time series can be used to predict a driver time series[27] (see *Methods*). If this prediction is successful beyond some appropriate null hypothesis (*Methods*), we take it as evidence of dynamical coupling. Applying CCM in expanding time windows, we find a significant dynamical influence of *ASI* on $SCOR_{ara}$ in the Ordovician - Jurassic (Fig. 2c), implying a causal link between aragonite-calcite sea conditions and $SCOR_{ara}$ in this part of the record. Following a maximum in the early Jurassic (Sinemurian), the CCM prediction skill decreases gradually until the Early Cretaceous and remains low thereafter. This decline indicates a weakening influence of ASI on the success of marine calcifiers towards the present.

92 Our findings corroborate the hypothesis of a decreasing environmental influence on marine
93 calcifiers' success. The correlation of aragonite-calcite seas and the success of aragonitic
94 calcifiers decreased chiefly in two episodes: Around the Carboniferous-Permian boundary,
95 and in a second episode centred in the Middle Jurassic (Fig 2). Permian seawater had an
96 unusually high $CaCO_3$ saturation[12,29]. All else being equal, higher $CaCO_3$ saturation facilitates
97 calcification[30] and tends to shift the $CaCO_3$ polymorph balance in favour of calcite[31].
98 Consequently, calcifiers with a calcitic skeleton performed better than predicted by *ASI* when
99 the $CaCO_3$ saturation state rose in the Permian. Calcitic taxa, particularly brachiopods,
100 became more successful across the Carboniferous – Permian boundary (Supplementary
101 Fig. S8, a detailed discussion of the relative success of the major taxonomic groups of marine
102 calcifiers is provided in the Supplementary Materials). The influence of *ASI* on $SCOR_{ara}$
103 decreased but their correlation remained positive within the Permian (Fig. 2b, Table 1).
104 Although $CaCO_3$ saturation state probably remained high during the Triassic[32], *ASI* continued
105 to affect $SCOR_{ara}$ in the early Mesozoic, but not thereafter.

106 ## The role of calcifying plankton

107 In the mid-Mesozoic, the Earth-Life system was revolutionised by the rise of calcifying
108 plankton[12]. Before the widespread occurrence of planktonic calcifiers, $CaCO_3$ precipitation
109 was largely confined to the continental shelves and linked to the success of benthic calcifiers
110 such as corals and brachiopods. The evolutionary success of calcifying plankton, especially of
111 coccolithophores[33], shifted the carbonate factory from the shelves to the open ocean.
112 Calcareous tests sink to the ocean floor and either dissolve or accumulate, depending on the
113 local $CaCO_3$ saturation state. Since the proliferation of planktonic calcifiers, changes in the
114 atmospheric and oceanic CO_2 content have been compensated on geologically short time

115 scales by increased $CaCO_3$ deposition or dissolution in the deep sea[34]. The evolutionary impact
116 of episodes of severe climatic change with associated ocean acidification such as the
117 Palaeocene-Eocene Thermal Maximum has been less severe than comparable events in the
118 Palaeozoic and early Mesozoic[35,36], possibly a consequence of the increased ocean
119 buffering[12,37]

120 Producing a skeleton out of *sync* with aragonite-calcite sea conditions may be costly especially
121 when $CaCO_3$ secretion is impeded by ocean acidification. Enhanced ocean buffering after the
122 proliferation of calcifying plankton can explain the diminished response of marine calcifiers
123 to changing aragonite-calcite sea conditions after the mid-Jurassic. Several key events in the
124 evolution of calcifying plankton fall into the Middle – Late Jurassic. Planktonic foraminifera
125 first appear in the fossil record during the Lower Jurassic, but the first known deep water
126 carbonate oozes composed of planktonic foraminifera date back to the Middle Jurassic[38,39].
127 The thick-walled coccolithophore genus *Watznaueria* diversified in the early Middle Jurassic,
128 resulting in an increase of coccolith flux to the sediment by two orders of magnitude[40].
129 Nannofossil deposits from the Tethys ocean show that coccolithophores colonised the open
130 ocean during the Late Jurassic and became abundant enough to affect the marine carbonate
131 system[41].

132 ## A new evolutionary regime

133 Beyond skeletal mineralogy, there is evidence for a wider regulatory change of evolutionary
134 patterns and environmental state shifts in the mid-Phanerozoic. Devastating extinctions in
135 the Late Permian – early Mesozoic overturned the taxonomic composition of marine
136 calcifiers[36,42] and favoured the survival of active and physiologically buffered animals[28,43]. As
137 a consequence, the dominant, modern marine biota are less vulnerable to abiotic stressors

than their Palaeozoic counterparts[43], and individual energy budgets of bivalves and gastropods increased throughout the early Mesozoic[3,5]. This rise in available metabolic energy may have helped absorb the cost of secreting a shell out of *sync* with aragonite-calcite sea conditions.

The Mesozoic rise of plankton such as foraminifera[38], coccolithophores, and dinoflagellates[44] had an additional effect on the bio-geosphere: tests of phytoplankton act as ballast, increasing its sinking velocity and increasing the depth at which organic carbon is oxidised, which in turn can explain the much lower prevalence of anoxia on Mesozoic and Cenozoic shelves[45]. Increasing oxygenation of shallow ocean water is indicated from the Jurassic onwards by iodine-to-calcium ratios[46] (Fig. 1f). Well-oxygenated shelves stabilise the carbon cycle by reducing the impact of sea level changes on the burial capacity of organic carbon[13], thus decreasing the potential for catastrophic environmental change. Increasing oxygen availability also allows for higher metabolic rates and more active modes of life in the shelf biota, as has been inferred for the mid-Mesozoic[47] and may have increased the pace of escalation in evolution[48]. The onset of a persistent diversity rise in the Middle Jurassic agrees with this interpretation (Fig. 1g).

Our results specify the long-held notion that "the evolutionary milieu in which taxa find themselves changed substantially" from the Palaeozoic to the modern world[49]: We found a prominent decrease in environmental influence on the ecological success of marine calcifiers, although some 80 million years after the end of the Palaeozoic. This regime shift was caused by a number of abiotic and biotic revolutions in the Earth-Life system. Of all the factors contributing to this pattern, the onset of the modern carbon cycle via deep-sea $CaCO_3$ sedimentation was likely the most consequential for marine calcifying organisms. The high-

level taxonomic composition of marine life changed towards a “modern” biota after the end-Permian catastrophe[1], but the Palaeozoic evolutionary regime may have persisted well into the Mesozoic.

References

1 Alroy, J. The shifting balance of diversity among major marine animal groups. *Science* **329**, 1191-1194 (2010).

2 Bambach, R. K., Knoll, A. H. & Sepkoski, J. J. Anatomical and ecological constraints on Phanerozoic animal diversity in the marine realm. *Proceedings of the National Academy of Sciences* **99**, 6854-6859 (2002).

3 Finnegan, S., McClain, C. M., Kosnik, M. A. & Payne, J. L. Escargots through time: an energetic comparison of marine gastropod assemblages before and after the Mesozoic Marine Revolution. *Paleobiology* **37**, 252-269 (2011).

4 Heim, N. A., Knope, M. L., Schaal, E. K., Wang, S. C. & Payne, J. L. Cope’s rule in the evolution of marine animals. *Science* **347**, 867-870 (2015).

5 Payne, J. L., Heim, N. A., Knope, M. L. & McClain, C. R. Metabolic dominance of bivalves predates brachiopod diversity decline by more than 150 million years. *Proc. R. Soc. B* **281**, 20133122 (2014).

6 Ausich, W. I. & Bottjer, D. J. Tiering in Suspension-Feeding Communities on Soft Substrata throughout the Phanerozoic. *Science* **216**, 9 (1982).

7 Vermeij, G. J. The Mesozoic marine revolution: evidence from snails, predators and grazers. *Paleobiology* **3**, 245-258 (1977).

8 Vermeij, G. J. *Evolution and escalation: an ecological history of life*. (Princeton University Press, 1987).

9 Aberhan, M., Kiessling, W. & Fürsich, F. T. Testing the role of biological interactions in the evolution of mid-Mesozoic marine benthic ecosystems. *Paleobiology* **32**, 259-277 (2006).

10 Sandberg, P. A. An oscillating trend in Phanerozoic non-skeletal carbonate mineralogy. *Nature* **305**, 19-22 (1983).

11 Veizer, J., Godderis, Y. & François, L. M. Evidence for decoupling of atmospheric CO_2 and global climate during the Phanerozoic eon. *Nature* **408**, 698-701 (2000).

12 Ridgwell, A. A Mid Mesozoic Revolution in the regulation of ocean chemistry. *Marine* Geology **217**, 339-357 (2005).

13 Bachan, A. *et al.* A model for the decrease in amplitude of carbon isotope excursions across the Phanerozoic. *American Journal of Science* **317**, 641-676 (2017).

14 Alroy, J. Accurate and precise estimates of origination and extinction rates. *Paleobiology* **40**, 374-397 (2014).

15 Balthasar, U. & Cusack, M. Aragonite-calcite seas—Quantifying the gray area. *Geology* **43**, 99-102 (2015).

16 Hardie, L. A. Secular variation in seawater chemistry: An explanation for the coupled secular variation in the mineralogies of marine limestones and potash evaporites over the past 600 my. *Geology* **24**, 279-283 (1996).

17 Higuchi, T., Shirai, K., Mezaki, T. & Yuyama, I. Temperature dependence of aragonite and calcite skeleton formation by a scleractinian coral in low mMg/Ca seawater. *Geology* **45**, 1087-1090 (2017).

18 Ramajo, L., Rodríguez-Navarro, A. B., Duarte, C. M., Lardies, M. A. & Lagos, N. A. Shifts in shell mineralogy and metabolism of Concholepas concholepas juveniles along the Chilean coast. *Marine and Freshwater Research* **66**, 1147-1157 (2015).

19 Ries, J. Review: geological and experimental evidence for secular variation in seawater Mg/Ca (calcite-aragonite seas) and its effects on marine biological calcification. *Biogeosciences* **7**, 2795 (2010).

20 Harper, E. M., Palmer, T. J. & Alphey, J. Evolutionary response by bivalves to changing Phanerozoic sea-water chemistry. *Geological Magazine* **134**, 403-407 (1997).

21 Porter, S. Calcite and aragonite seas and the *de novo* acquisition of carbonate skeletons. *Geobiology* **8**, 256-277 (2010).

22 Demicco, R. V., Lowenstein, T. K., Hardie, L. A. & Spencer, R. J. Model of seawater composition for the Phanerozoic. *Geology* **33**, 877-880 (2005).

23 Veizer, J. & Prokoph, A. Temperatures and oxygen isotopic composition of Phanerozoic oceans. *Earth-Science Reviews* **146**, 92-104 (2015).

24 Hannisdal, B., Henderiks, J. & Liow, L. H. Long-term evolutionary and ecological responses of calcifying phytoplankton to changes in atmospheric CO_2. *Global Change Biology* **18**, 3504-3516 (2012).

25 Kiessling, W., Aberhan, M. & Villier, L. Phanerozoic trends in skeletal mineralogy driven by mass extinctions. *Nature Geoscience* **1**, 527-530 (2008).

26 Foote, M., Crampton, J. S., Beu, A. G. & Nelson, C. S. Aragonite bias, and lack of bias, in the fossil record: lithological, environmental, and ecological controls. *Paleobiology* **41**, 245-265 (2015).

27 Sugihara, G. *et al.* Detecting causality in complex ecosystems. *science*, 1227079 (2012).

28 Knoll, A. H., Bambach, R. K., Payne, J. L., Pruss, S. & Fischer, W. W. Paleophysiology and end-Permian mass extinction. *Earth and Planetary Science Letters* **256**, 295-313 (2007).

29 Grotzinger, J. P. & Knoll, A. H. Anomalous carbonate precipitates: is the Precambrian the key to the Permian? *Palaios*, 578-596 (1995).

30 Langdon, C. *et al.* Effect of calcium carbonate saturation state on the calcification rate of an experimental coral reef. *Global Biogeochemical Cycles* **14**, 639-654 (2000).

31 De Choudens-Sanchez, V. & Gonzalez, L. A. Calcite and aragonite precipitation under controlled instantaneous supersaturation: elucidating the role of $CaCO_3$ saturation state and Mg/Ca ratio on calcium carbonate polymorphism. *Journal of Sedimentary Research* **79**, 363-376 (2009).

32 Webb, G. E. Was Phanerozoic reef history controlled by the distribution of non-enzymatically secreted reef carbonates (microbial carbonate and biologically induced cement)? *Sedimentology* **43**, 947-971 (1996).

33 Bown, P. R., Lees, J. A. & Young, J. R. in *Coccolithophores* 481-508 (Springer, 2004).

34 Ridgwell, A. & Zeebe, R. E. The role of the global carbonate cycle in the regulation and evolution of the Earth system. *Earth and Planetary Science Letters* **234**, 299-315 (2005).

35 Clapham, M. E. & Renne, P. R. Flood Basalts and Mass Extinctions. *Annual Review of Earth and Planetary Sciences* **47** (2019).

36 Wignall, P. B. *The Worst of Times: How Life on Earth Survived Eighty Million Years of Extinctions*. (Princeton University Press, 2015).

37 Zeebe, R. E. & Westbroek, P. A simple model for the $CaCO_3$ saturation state of the ocean: The “Strangelove,” the “Neritan,” and the “Cretan” Ocean. *Geochemistry, Geophysics, Geosystems* **4** (2003).

38 Hudson, W., Hart, M. B. & Smart, C. W. Palaeobiogeography of early planktonic foraminifera. *Bulletin de la Societé géologique de France* **180**, 27-38 (2009).

39 Hart, M. B., Hudson, W., Smart, C. W. & Tyszka, J. A reassessment of ‘Globigerina bathoniana’Pazdrowa, 1969 and the palaeoceanographic significance of Jurassic planktic foraminifera from southern Poland. *Journal of Micropalaeontology* **31**, 97-109 (2012).

40 Suchéras-Marx, B. *et al.* Impact of the Middle Jurassic diversification of Watznaueria (coccolith-bearing algae) on the carbon cycle and δ 13 C of bulk marine carbonates. *Global and Planetary Change* **86**, 92-100 (2012).

41 Roth, P. H. Mesozoic palaeoceanography of the North Atlantic and Tethys oceans. *Geological Society, London, Special Publications* **21**, 299-320 (1986).

42 Alroy, J. Dynamics of origination and extinction in the marine fossil record. *Proceedings of the National Academy of Sciences* **105**, 11536-11542 (2008).

43 Clapham, M. E. Organism activity levels predict marine invertebrate survival during ancient global change extinctions. *Global change biology* **23**, 1477-1485 (2017).

44 Falkowski, P. G. *et al.* The evolution of modern eukaryotic phytoplankton. *Science* **305**, 354-360 (2004).

45 Meyer, K., Ridgwell, A. & Payne, J. The influence of the biological pump on ocean chemistry: implications for long-term trends in marine redox chemistry, the global carbon cycle, and marine animal ecosystems. *Geobiology* **14**, 207-219 (2016).

46 Lu, W. *et al.* Late inception of a resiliently oxygenated upper ocean. *Science* **361**, 174-177, (2018).

47 Vermeij, G. J. Escalation and its role in Jurassic biotic history. *Palaeogeography, Palaeoclimatology, Palaeoecology* **263**, 3-8 (2008).

48 Vermeij, G. J. On escalation. *Annual Review of Earth and Planetary Sciences* **41**, 1-19 (2013).

49 Foote, M. Origination and extinction components of taxonomic diversity: Paleozoic and post-Paleozoic dynamics. *Paleobiology* **26**, 578-605 (2000).

Corresponding author

Correspondence and requests for materials should be addressed to Kilian Eichenseer (kilian.eichenseer@plymouth.ac.uk).

Acknowledgements

This project was supported by the University of Plymouth (K.E., U.B., C.W.S. and J.S.) , by the Trond Mohn Foundation (funding to K.A.H.) and by the Deutsche Forschungsgemeinschaft (KI 806/16-1, funding to W.K.). We thank all contributors to the Paleobiology Database, and David Diego for discussions on pullback attractor formalism and CCM interpretations. We are grateful to James Crampton, Ashleigh Hood for their comments on an earlier version of this manuscript. This is Paleobiology Database publication no. 344.

Author contributions

K.E., U.B., W.K. and C.W.S. designed the study. J.S. developed and implemented the Bayesian changepoint regression analysis. K.A.H. performed the convergent cross mapping analysis. K.E. carried out all other data analysis and wrote the initial manuscript draft, and all authors contributed substantially to its improvement.

Competing interests

The authors declare no competing interests.

Figures

Figure 1

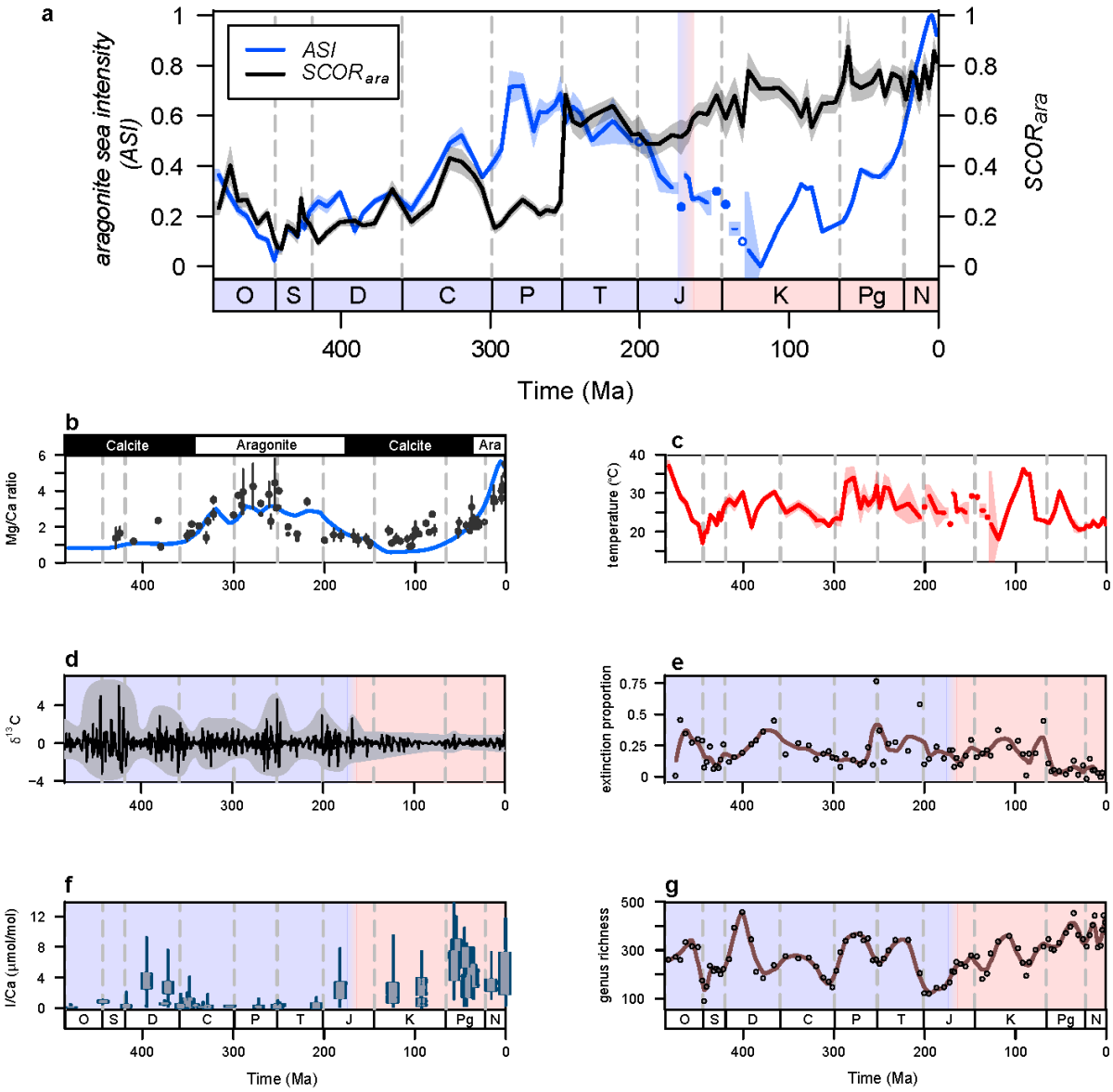

Figure 1: Environmental and biotic changes across the Ordovician – Neogene

(a) *ASI* (aragonite sea intensity, blue) and $SCOR_{ara}$ (relative Summed Common species Occurrence Rate of aragonitic genera, black), in 85 Ordovician – Pleistocene stages. Shaded areas represent 2 standard errors around the mean with the *ASI* error envelope being based on the temperature component (*Methods*). Stages

with only one measurement are drawn as solid dots, stages without observations (circles) have been averaged from the neighboring stages.

Legend: O = Ordovician, S = Silurian, D = Devonian, C = Carboniferous, P = Permian, T = Triassic, J = Jurassic, K = Cretaceous, Pg = Palaeogene, N = Neogene and Quaternary, Ma = Million years ago. The blue – red transitions and the vertical bar mark the time when the relationship between *ASI* and $SCOR_{ara}$ decreased most strongly (See Fig. 2b, c).

(b) Modelled Mg/Ca ratio from ref. 22 (blue line) and a compilation of Mg/Ca proxy data (black dots, see Supplementary Materials S1). The bar at the top delineates calcite and aragonite sea intervals as predicted by ref. 16.

(c) Mean stage-level tropical shallow water temperatures calculated from oxygen isotope measurements compiled in ref. 23. Stages with only one measurement are drawn as solid dots, stages without observations have been averaged from the neighbouring stages and are shown as circles. Shaded areas represent 2 standard errors around the mean.

(d) Periodic changes in the envelope of third-order $\delta^{13}C$ variations, reprinted from ref. 13 with permission of the American Journal of Science. The grey area highlights the variability.

(e) Genus-level, sampling-standardised extinction proportions (circles, see *Methods*) with long-term trend line (brown; LOESS regression with a smoothing span of 0.1).

(f) Box plots showing the variability of iodine-to-calcium (I/Ca) ratios from shallow water carbonates within sampling localities, reprinted from ref. 46 with permission from

AAAS. I/Ca ratios are considered a proxy for oxygenation, with higher I/Ca ratios indicating better oxygenation.

(g) Sampling-standardised marine genus-level diversity (circles, see *Methods*) with long-term trend line (brown; LOESS regression with a smoothing span of 0.1).

Figure 2

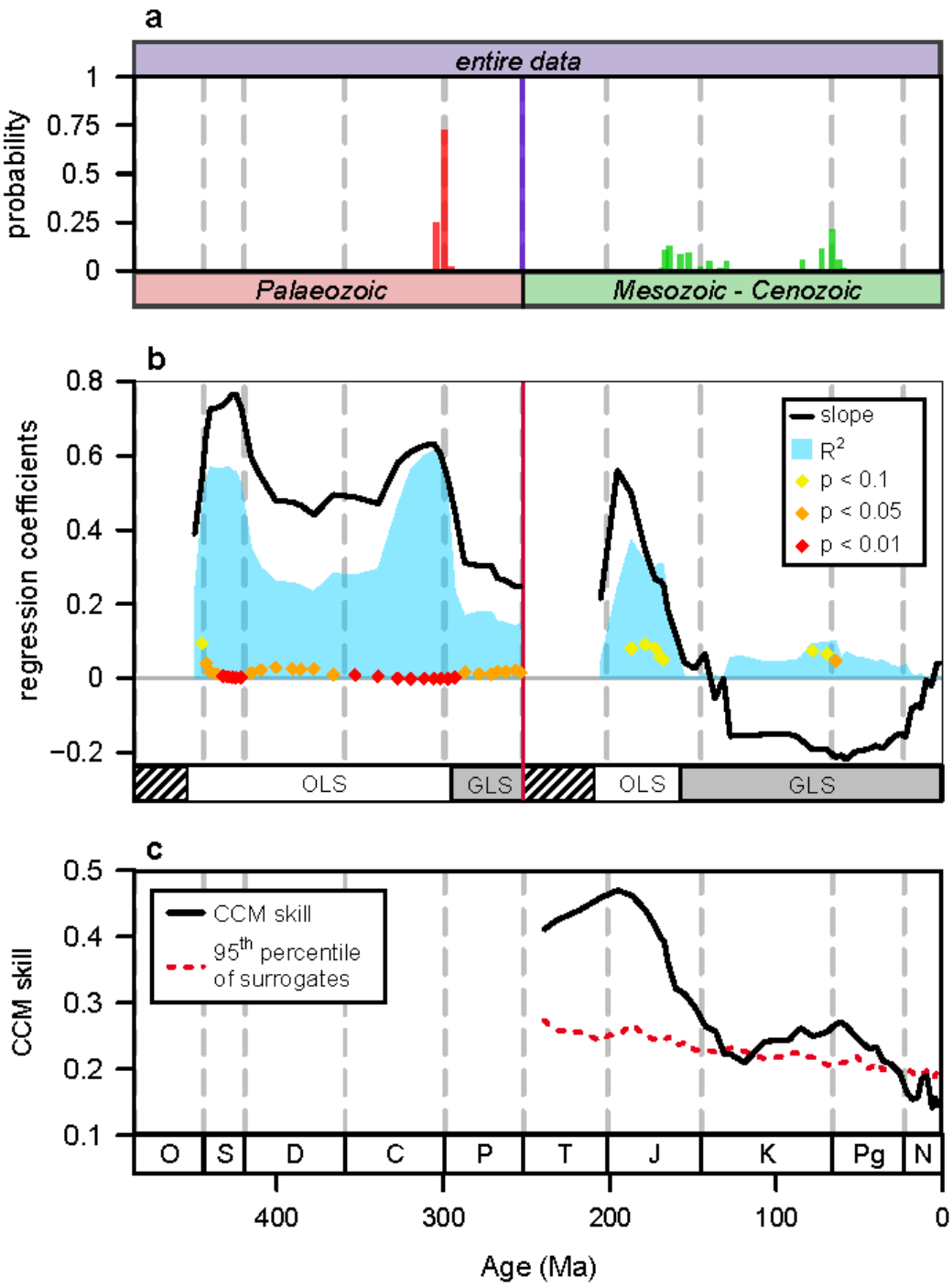

334

335 **Figure 2: Changing relationship of *SCOR*$_{ara}$ and *ASI*.**

336 (a) Bayesian posterior probabilities for changes in the linear regression of *SCOR*$_{ara}$ against *ASI*

337 for the entire time series (purple bar), the Palaeozoic (red) and the Triassic – Pleistocene

(green). The strength of correlation between $SCOR_{ara}$ and *ASI* changed around the Carboniferous – Permian boundary and at the Permian – Triassic boundary, whereas no distinct point of change is found in the Mesozoic – Cenozoic time series.

(b) Linear models of $SCOR_{ara}$ against *ASI* in windows of increasing length for the Palaeozoic and for the Mesozoic – Cenozoic. Expanding windows start with the first six stages and all data are plotted at the last stage of the respective window. Black line = slope; blue area = R^2; diamonds = p-values; only p-values < 0.1 are shown. The boxes at the bottom of the graph indicate the gap for the first five stages (hatched pattern), and whether linear models were generated using ordinary least squares (OLS), or generalised least squares (GLS, *see Methods*). These results demonstrate a strong positive correlation between $SCOR_{ara}$ and *ASI* for the Palaeozoic time series, and a strong, although less robust positive correlation in the early Mesozoic that weakens with the inclusion of data from the Middle Jurassic onwards.

(c) Predicting *ASI* from $SCOR_{ara}$ with convergent cross mapping (CCM) for expanding time series. All included time series start with the first Ordovician stage and all data are plotted at the last stage of their respective window. The CCM prediction skills (solid black line) can be interpreted as the strength of dynamical influence of *ASI* on $SCOR_{ara}$. The dashed red line shows the 95^{th} percentile of 500 random surrogate time series, which we take as a significance criterion. Time windows shorter than the Ordovician – Middle Triassic did not pass the CCM convergence test and were not included (*see Methods*). The CCM skill shows a sustained drop when Jurassic – Early Cretaceous stages are added, which implies a continuously weakening dynamical influence of *ASI* on $SCOR_{ara}$.

Tables

Table 1: Linear models with GLS

(d) Generalised least squares linear models of $SCOR_{ara}$ against *ASI* in the entire data set and in temporal subsets. N denotes the number of observations, $\boldsymbol{\varepsilon}$ denotes the error term of the regression, with AR indicating autoregressive errors and *ind.* indicating independent errors. ϕ denotes the autocorrelation of the error at lag = 1. In models with autocorrelated error terms, R^2 is calculated from the log-likelihoods of the model and the corresponding null model (*Methods*). Models with independent errors are equivalent to an ordinary least squares linear model.

	N	$\boldsymbol{\varepsilon}$	**ϕ**	**Intercept**	**Slope**	**R^2**	***p***
entire data set	85	AR	0.93	0.45	0.05	0.00	0.70
Palaeozoic	38	AR	0.57	0.13	0.25	0.15	**0.017**
Ordovician - Carboniferous	29	*ind.*	-	0.07	0.60	0.59	**< 0.001**
Permian	9	*ind*.	-	0.05	0.28	0.68	**0.006**
Mesozoic - Cenozoic	47	AR	0.68	0.65	0.04	0.00	0.68

Methods

Fossil and palaeoenvironmental data were grouped into 85 Ordovician to Pleistocene geological stages. To achieve more uniform stage durations, we combined stages shorter than 1 million years (myr) with neighbouring stages (Table S4). Consequently, the two Early Triassic stages were combined, as were the four Pleistocene stages. All analyses were carried out in R, version 3.4.1[50]

Fossil data. We used the Paleobiology Database (PBDB, https://paleobiodb.org/) to assess the global fossil record of marine calcifiers. The PBDB records occurrences of fossil organisms and the geological setting in which they were preserved. For our analysis, we relied on internal PBDB information on stratigraphy, taxonomy, mineralogy, life habits, preservation, lithification, and palaeocoordinates (Table S3). All Phanerozoic occurrence data were downloaded on 24 January 2017 with standard settings. Cambrian occurrences were later omitted as *ASI* could only be calculated in the Ordovician – Pleistocene due to the insufficient Cambrian palaeotemperature record. We also excluded occurrences from non-marine settings and occurrences that could not be assigned with confidence to a geological stage. We only included occurrences that were identified to genus level and that could be reliably assigned to an invertebrate animal phylum, Foraminifera, Chlorophyta, Rhodophyta, or calcifying "Problematica". Occurrences of plankton (coccolithophores, planktonic foraminifera, planktonic gastropods or planktonic tentaculites) were omitted. We followed the classification of skeletal mineralogy in the PBDB and considered calcifiers as "aragonitic" if their dominant mineralogy was aragonite and no secondary mineral was listed. The skeletal mineralogies recorded in the PBDB are based on the protocol described in ref. 25, from which we deviated in few exceptions – labechiid and Palaeozoic chaetetid sponges were classified as possessing a high Mg calcite skeleton (Balthasar *et al.*, unpublished).

As aragonite is thermodynamically instable at Earth surface conditions and eventually dissolves or recrystallizes to calcite, aragonite has a lower preservation potential than calcite[26,51]. Most occurrences of aragonite preservation are therefore concentrated in the youngest stages. We

minimized this time-dependant bias by excluding all occurrences from collections with aragonite preservation and unlithified sediments, but kept the 19 % of data which had no information on their preservation recorded to avoid excessive loss of fossil data (see Supplementary Text S3). Barring some potential undeclared occurrences of aragonite preservation, the record of aragonitic taxa used herein thus consists of specimens that have been recrystallized to the stable calcite polymorph or that have been preserved in another way, e.g. by silicification.

Aragonite sea intensity (ASI). We developed a proxy for the degree to which aragonite precipitation is favoured relative to calcite precipitation in the non-biogenic environment based on the joint influence of temperature (*T*) and the Mg/Ca ratio on $CaCO_3$ formation in experiments[52]. We conducted a multiple linear regression of the mole percent of aragonite present in every experiment against the temperature and Mg/Ca ratio under which the experiments were conducted (see figure 1 in ref. 15). We only used experiments that produced > 1 % calcite and > 1 % aragonite. This yields the equation

(1) $$ASI = -119.61 + 46.57 \times \frac{Mg}{Ca} + 4.30 \times T$$

To infer past *ASI* for the Ordovician – Pleistocene, palaeotemperatures were calculated from a Phanerozoic $\delta^{18}O$ compilation[23], including only measurements from fossil brachiopods, bivalves and planktonic foraminifera from 35° south to 35° north, because measurements from higher latitudes are unavailable for most of the Phanerozoic. For the $\delta^{18}O$ (‰ PDB) to *T*(°C) transfer function, we calculated palaeotemperatures assuming a Phanerozoic trend of increasing $\delta^{18}O$ as in equation (2) from ref. 23. The Mg/Ca ratio ratios were taken from a Phanerozoic model of seawater composition and digitised from fig. 2.A of ref. 22 in steps of 2 million years using the R package *digitize*. For the Mg/Ca data, the mean from all observations falling into a geological stage was taken. *ASI* was calculated with average Mg/Ca data and with every individual temperature observation using equation (1). Mean and standard error of all *ASI* were calculated for each stage, and the resulting *ASI* was normalised to values between 0 and 1. No temperature data was available for the Hettangian and for the Hauterivian stage. We

calculated *ASI* for these stages with the mean temperature of the two neighbouring stages, respectively.

$SCOR_{ara}$. Evolutionary success is widely assessed by diversity. Although species diversity and abundance of higher taxonomic ranks or ecological groups are tightly coupled[53], we prefer a direct measure of occupancy to assess the ecological success of individual genera. We apply the Summed Common species Occurrence Rate (SCOR), which is driven by the most widespread and common taxa[24]. SCOR reflects the actual abundance of a group of taxa with good accuracy[54]. The cumulative SCOR of a set of *m* genera is calculated as

$$(2)\ \mathrm{SCOR} = \sum_{i=1}^{m} -\ln\left(1 - \frac{y_i}{k}\right)$$

where genus *i* is present in y_i subsets out of a total of *k* occupied localities. We defined a locality as a cell in a global penta-hexagonal grid with 6240 hexagonal and 12 pentagonal grid cells, with an area of ca. 40,800 km^2. The grid was generated using the hexagrid() function in the icosa package[55]. The contribution of a genus to SCOR thus depends solely on the number of cells it was sampled in. Repeated sampling within a cell does not increase SCOR. $SCOR_{ara}$ reflects the ecological occupancy of aragonitic taxa, relative to all calcifiers occurring at k_{all} localities. $SCOR_{ara}$ is generated by dividing the SCOR of aragonitc taxa with $k = k_{all}$ by the SCOR of all calcifying genera, again with $k = k_{all}$. To get the relative success of major taxonomic groups, we divided the group SCOR by the SCOR of all calcifiers. For every stage, we calculated SCOR using all genera recorded in the PBDB fossil data recorded in that respective stage.

We calculated the variance of any SCOR metric with the delta method[24,56]

$$(3)\ \mathrm{Var}(\mathrm{SCOR}) = \sum_{i=1}^{m} \frac{\frac{y_i}{k}}{\left(1-\frac{y_i}{k}\right)*k}$$

and can approximate the variance of $SCOR_{ara}$ using the means and variance of aragonitic SCOR and the SCOR of all calcifiers, assuming they are independent:

436 (4) $\mathrm{Var}(\mathrm{SCOR}_{ara}) = (\frac{aragonitic\ SCOR}{all\ calcifier\ SCOR})^2 \times \left(\frac{Var(aragonitic\ SCOR)}{aragonitic\ SCOR} + \frac{Var(all\ calcifier\ SCOR)}{all\ calcifier\ SCOR}\right)$.

437 **Bayesian change point regression analysis.** The relationship of *ASI* and $SCOR_{ara}$ changed through time.
438 We developed statistical methodology to identify change points. In particular, we performed
439 inference in the Bayesian framework about the unknown parameters of the model $y_i \sim N(\mu_i, \sigma_i^2)$,
440 $i = 1,\ldots,n$, independently, in which n is the overall sample size and

441 (5) $\mu_i = \begin{cases} \alpha_1 + \beta_1 x_i & i = 1, \ldots, n_1 \\ \sum_{j=1}^{2} \alpha_j + \sum_{j=1}^{2} \beta_j x_i & i = n_1 + 1, \ldots, n \end{cases}$

442 This model allows a distinct linear relationship between y_i and the covariate x_i in a first and second
443 part of the time series. The parameter α_2 and β_2 represent the additional intercept and slope in the
444 second part, added to α_1 and β_1 of the first part. log σ_i is defined in a similar way, allowing for a
445 different relationship between the standard deviation σ_i and the covariate x_i in each time series part.

446 In the Bayesian framework, it is necessary to specify prior distributions for all unknown parameters.
447 We adopted normal priors with very high variances for all intercept and slope parameters. For the
448 change point n_1, we adopted a discrete uniform prior across integer values from 5 to $n - 5$, implying
449 that the change point divides the time series into two sections with at least five data points each. This
450 prior distribution expresses considerable uncertainty about the position of the change point before
451 seeing the data. As it is impossible to handle the posterior distribution of all these parameters
452 analytically, we followed the standard approach of sampling from this distribution using a Markov
453 chain Monte Carlo (MCMC) algorithm[57]. To do this we used the jags program[58], accessed in R through
454 the R2jags package[59]. Our posterior inference is based on 100,000 iterations of the MCMC algorithm,
455 half of which were discarded as burn-in.

456 After inferring a first change point at the Permian-Triassic boundary, we split the data set into a
457 Palaeozoic part and a Mesozoic – Cenozoic part. In each of the two parts, we estimated additional
458 change points with the method described above.

Generalised least squares. Linear regression with ordinary least squares (OLS) of the form

$$y = \alpha + \beta x + \varepsilon \quad (6)$$

assumes that the errors ε are independent between observations. For our data, the residuals of an OLS linear model of $SCOR_{ara}$ against *ASI* are autocorrelated, which suggests that this assumption of independent errors does not hold. Generalised least square regression (GLS) can incorporate autoregressive errors and thus allows us to test for linear relationships between autocorrelated time series[60]. Autocorrelated errors ε of order p can be modelled as

$$\varepsilon_i = \sum_{j=1}^{p} \phi_j \, \varepsilon_{i-j} + \delta_i \quad (7)$$

with $\delta_i \sim N(0,\sigma^2)$ independently, in which σ is the standard deviation. We created linear models with independent and with autocorrelated error terms of the first order using the gls() function of the nlme R package[61], performing maximum likelihood estimation by specifying gls(…, method = "ML"). For model selection we compared pairs of models with and without autoregressive errors using a likelihood ratio test[62], implemented using the anova.gls() function. We selected the more complicated model only if the associated p-value was < 0.05 and the likelihood ratio was > 1. In a few instances, models with autocorrelated errors estimated $\phi < 0$, which we attributed to model overfitting. In these cases, we chose the model without autocorrelation.

As a goodness-of-fit measure for GLS models, we calculated the likelihood ratio test R^2 as

$$R^2 = 1 - \exp\left(-\frac{2}{m}(\log L_M - \log L_0)\right) \quad (8)$$ [63,64],

with m being the number of observations, $\log L_M$ being the log-likelihood of the model, and $\log L_0$ being the log-likelihood of the null model of the form $y = 1 + \varepsilon$, with ε being the error as in equation (7).

We take 0.05 as the alpha level for the statistical significance of linear regressions.

Regression in expanding windows. We assessed the changing strength of a relationship between *ASI* and $SCOR_{ara}$ through time by calculating linear models in windows of expanding length. Due to the

severe increase of $SCOR_{ara}$ across the Permian-Triassic boundary, calculating the linear relationship across the entire data set may be misleading. Instead, linear models were formulated separately in the Palaeozoic and Mesozoic-Cenozoic. In both cases, the shortest window considered comprised the first six data points, while the longest window had 38 points in the Palaeozoic and 47 points in the Mesozoic – Cenozoic. In every window, an OSL and a GLS model was fitted, with autoregressive errors of the first order incorporated into the GLS model. GLS models were used from the first window onwards in which ϕ was positive and a likelihood ratio test comparing the OLS and the GLS model produced a *p*-value < 0.05.

Convergent cross mapping. The success of marine calcifiers may be influenced by environmental parameters other than climate and ocean chemistry, as well as biotic interactions and chance. It is therefore possible that a causal connection between ASI and $SCOR_{ara}$ exists even when no linear relationship is detected. We test for this possibility using CCM, a model-free time series analysis method based in dynamical systems theory that can detect causal coupling in nonlinear and even chaotic systems[27]. It asserts that if two processes are causally linked, then information about the driver variable can be recovered from the response variable[27]. CCM indirectly measures the dynamical influence of the driver variable on the response variable by quantifying the extent to which a state space reconstruction (time delay embedding) of the response variable can be used to predict the driver time series. A description of the algorithm can be found in the Supplementary Materials (S2).

To test for a temporally variable influence of *ASI* on $SCOR_{ara}$, we performed CCM analysis on expanding time windows on the stage level data, under the assumption that these coarse-grained data contain sufficient dynamical information about Phanerozoic Earth system dynamics (see Supplementary Materials S2). We used the rEDM R package[65] to perform CCM analyses for the main paper. Because of the limited number of time series points, we used embedding dimension 2 and embedding lag 1, with zero temporal exclusion radius in the predictions due to the coarse temporal resolution of the data. For a given time window, the CCM analysis is convergent if prediction skill

increases with increasing library size (Supplementary Materials S2). If convergence is achieved, for each time window of length L, we report the median CCM skill for 500 bootstrapped samples at a library size L. In addition, to assess the significance of the results, we used surrogate testing with randomly shuffled surrogates[66]. The analysis for a given time window was considered significant if the median prediction skill at the largest library size exceeded the 95th percentile of the median prediction skills obtained for an ensemble of 500 surrogate CCM analyses (dashed, red line in Fig. 2c), where each surrogate realization, the driver time series is replaced by a randomly shuffled version of itself.

Diversity dynamics. We calculated second-for-third extinction proportions[67] using classical rarefaction[14,68] with a sampling quota of 500 occurrences per stage and took the mean extinction proportions over 100 subsampling trials. A sampling-standardised diversity curve was generated with shareholder-quorum subsampling[1] by taking the mean of 100 subsampling iterations, each with a quorum of 0.7. Following the recommendations in ref. 1, we relied on the reference-based singleton count, excluded the dominant genus from frequency calculations, and excluded the largest collection from the single-publication occurrence count. To control for short-term sampling variation, we used the corrected sampled-in-bin richness metric[69], except for the first and the last stage, in which no sampling correction could be made. A locally estimated scatterplot smoothing (LOESS) regression[70] has been calculated from these results using a smoothing span of 0.1. Extinction and diversity computations were performed using the divDyn R package[71].

Data availability

The data used to calculate $SCOR_{ara}$ are available from the Paleobiology Database at https://paleobiodb.org/. The data used to calculate aragonite sea intensity were taken from ref. 15, 22, and 23.

Code availability

The code used to generate the results can be accessed at https://figshare.com/articles/R_scripts_and_protocols/7199561.

Methods only References

50 R Core Team. R: A Language and Environment for Statistical Computing. *https://www.R-project.org/* (2017).

51 Cherns, L. & Wright, V. P. Quantifying the impacts of early diagenetic aragonite dissolution on the fossil record. *Palaios* **24**, 756-771 (2009).

52 Balthasar, U. *et al.* Relic aragonite from Ordovician–Silurian brachiopods: Implications for the evolution of calcification. *Geology* **39**, 967-970 (2011).

53 Madin, J. S. *et al.* Statistical independence of escalatory ecological trends in Phanerozoic marine invertebrates. *Science* **312**, 897-900 (2006).

54 Hannisdal, B., Haaga, K. A., Reitan, T., Diego, D. & Liow, L. H. Common species link global ecosystems to climate change: dynamical evidence in the planktonic fossil record. *Proc. R. Soc. B* **284**, 20170722 (2017).

55 Kocsis, Á. T. The R package icosa: Coarse resolution global triangular and penta-hexagonal grids based on tessellated icosahedra. R package version 0.9.81. *https://CRAN.R-project.org/package=icosa* (2017).

56 Casella, G. & Berger, R. L. *Statistical inference*. Vol. 2 (Duxbury Pacific Grove, CA, 2002).

57 Brooks, S., Gelman, A., Jones, G. & Meng, X.-L. *Handbook of markov chain monte carlo*. (CRC press, 2011).

58 Plummer, M. JAGS Version 3.3. 0 user manual. *International Agency for Research on Cancer, Lyon, France* (2012).

59 Su, Y. & Yajima, M. R2jags: Using R to run 'JAGS'. R package version 0.5–7. *https://CRAN.R-project.org/package=R2jags* (2015).

60 Faraway, J. J. *Linear models with R*. (CRC press, 2014).

61 Pinheiro, J. *et al.* nlme: Linear and Nonlinear Mixed Effects Models. R package version 3.1-131. *https://CRAN.R-project.org/package=nlme* (2017).

62 Davison, A. C. *Statistical models*. Vol. 11 (Cambridge University Press, 2003).

63 Kramer, M. R 2 statistics for mixed models. *Presented at the 17th Annual Kansas State University Conference on Applied Statistics in Agriculture, Manhattan, Kansas, 24–26 April* (2005).

64 Magee, L. R 2 measures based on Wald and likelihood ratio joint significance tests. *The American Statistician* **44**, 250-253 (1990).

65 Ye, H., Clark, A., Deyle, E., Keyes, O. & Sugihara, G. *rEDM: Applications of empirical dynamic modeling from time series.* R Package Version 0.5 7. *https://CRAN.R-project.org/package=rEDM* (2017).

66 Theiler, J., Eubank, S., Longtin, A., Galdrikian, B. & Farmer, J. D. Testing for nonlinearity in time series: the method of surrogate data. *Physica D* **58**, 77–94 (1992).

67 Alroy, J. A more precise speciation and extinction rate estimator. *Paleobiology* **41**, 633-639 (2015).

68 Sanders, H. L. Marine benthic diversity: a comparative study. *The American Naturalist* **102**, 243-282 (1968).

69 Alroy, J. *et al.* Phanerozoic trends in the global diversity of marine invertebrates. *Science* **321**, 97-100 (2008).

70 Cleveland, W. S., Grosse, E., Shyu, W. M., Chambers, J. M. & Hastie, T. Statistical models in S. *Local regression models*, Chapter 8 (1992).

71 Kocsis, Á. T., Reddin, C. J., Alroy, J. & Kiessling, W. The r package divDyn for quantifying diversity dynamics using fossil sampling data. *Methods in Ecology and Evolution* **10**, 735-743 (2019).